IEEE Access
Multidisciplinary ⋮ Rapid Review ⋮ Open Access Journal

Received 20 February 2025, accepted 2 March 2025, date of publication 5 March 2025, date of current version 13 March 2025.

Digital Object Identifier 10.1109/ACCESS.2025.3548116

RESEARCH ARTICLE

Energy Consumption Analysis of 5G C-V2X Sensor Sharing for Tele-Operated Driving

HANYOUNG PARK, (Graduate Student Member, IEEE), YONGJAE JANG, (Graduate Student Member, IEEE), KANGHYUN KO, AND JI-WOONG CHOI, (Senior Member, IEEE)

Department of Electrical Engineering and Computer Science, Daegu Gyeongbuk Institute of Science and Technology (DGIST), Daegu 42988, Republic of Korea

Corresponding author: Ji-Woong Choi (jwchoi@dgist.ac.kr)

This work was supported by the Institute of Information and Communications Technology Planning and Evaluation (IITP) Grant funded by Korean Government [Ministry of Science and ICT (MSIT)] under Grant RS-2024-00442085, Grant RS-2024-00398157, and Grant RS-2022-II221053.

ABSTRACT As autonomous driving technology advances, the demand for unmanned mobility applications continues to grow. However, due to the imperfections in current autonomous driving systems, incidents still occur, highlighting the challenges of full driverless services. Moreover, the computation of complex autonomous driving algorithms requires an on-board computing unit, which consumes a large amount of energy. To address these limitations, tele-operated driving (ToD) has emerged as a promising solution for enhancing autonomous intelligent transportation systems (ITS). By enabling remote entities, such as remote users or servers, to control vehicles and manage edge cases in autonomous driving, ToD combines the benefits of both unmanned mobility and human oversight. To support ToD service, a real-time sensor sharing system for vehicles is essential, and cellular vehicle-to-everything (C-V2X) communication is suitable for the required network connectivity. However, most research has not focused on high-volume data transmission, which is required for sensor sharing systems. Additionally, the energy consumption of C-V2X, which directly impacts the battery efficiency of electric vehicles (EVs) as an example, has not been thoroughly examined. In this paper, we propose an evaluation framework for energy consumption analysis of ToD. Based on this framework, we analyze the energy consumption of vehicle for sensor data transmission over 5G C-V2X under varying channel conditions and multi-user scenarios. We also investigate the extent to which using ToD is energy-saving compared to the energy consumption of an on-board high-performance computing unit. Our findings indicate that the uplink-based sensor sharing system is more energy-efficient than its sidelink-based counterpart. Additionally, sensor sharing for ToD can save more energy of the battery in the vehicle compared to relying on the high-performance on-board computing unit.

INDEX TERMS Unmanned mobility applications, tele-operated driving (ToD), sensor sharing, cellular vehicle-to-everything (C-V2X), energy consumption.

I. INTRODUCTION

Rapid advancement of smart vehicles, driven by various technological innovations, has significantly contributed to the development of intelligent transportation systems (ITS). According to the six levels of driving automation defined by the Society of Automotive Engineers (SAE), current technology has advanced to levels 2 and 3 [1]. These levels of autonomous driving are based on the proportion of the workload that the vehicle can handle, rather than the driver. If the vehicle assumes a greater portion of the driving workload, it would enhance the convenience of mobility for users. For example, ITS applications with higher levels of driving automation can offer unmanned services such as driverless taxis, unmanned delivery, and more [2], [3]. At this stage, consumers are increasingly demanding higher levels of autonomous driving, specifically level 4 and beyond, which require driverless capabilities [4]. However, current driving automation technologies still have challenges to support the desired unmanned mobility applications. For instance,

The associate editor coordinating the review of this manuscript and approving it for publication was Mauro Fadda.

© 2025 The Authors. This work is licensed under a Creative Commons Attribution 4.0 License.
For more information, see https://creativecommons.org/licenses/by/4.0/

an unmanned vehicle from Waymo stopped on a street in San Francisco, causing a traffic jam because one of its back doors was not completely closed [5]. Additionally, a Tesla vehicle running full self-driving software did not stop at a stop sign [6]. A driverless taxi from Cruise struck a pedestrian who had already been hit by another vehicle [7]. These incidents illustrate the incompleteness of technology related to driverless applications and services. Besides, high-performance computing units, such as central processing units (CPUs) and graphics processing units (GPUs), are required to operate complex algorithms for automotive services [8]. This demand implies additional energy consumption by high-performance computing units, and the extra energy requirements can affect the performance of electric vehicles due to their battery constraints.

As a result, remote driving services through tele-operated driving (ToD) are being considered as a potential solution to address the shortcomings of current autonomous technologies [9]. Remote users control the vehicle in real-time by using ToD, allowing them to complement the instability of autonomous driving. Remote users can intervene in driving scenarios and prevent incidents arising from corner cases, which driverless algorithms may struggle to manage [10]. The remote operation of ToD services also implies a reduced dependence on algorithms. Consequently, ToD suggests a diminished need for high-performance computing devices within the vehicle. Additionally, ToD enables the remote execution of specific driving tasks for non-automated vehicles, eliminating the need for an on-board driver. Therefore, ToD can leverage the inherent advantages of unmanned driving applications, such as freedom from spatial constraints, while simultaneously supporting desired future driverless services, including automated factory parking, valet parking, and remote driving in industrial zones or on public roads [11].

To support ToD services, a real-time sensor data sharing system between the vehicle and remote entities is a prerequisite. It requires wireless network connectivity, and vehicle-to-everything (V2X) communication has been considered as the solution to meet the demand for wireless connections. V2X comprises two main technologies: dedicated short range communication (DSRC) and cellular V2X (C-V2X) [12], [13]. Since DSRC is an application utilizing IEEE 802.11p wireless fidelity (Wi-Fi), it has drawbacks such as short coverage and limited network connectivity, making it an unsuitable technology for ToD. To reduce the performance gap between DSRC and C-V2X, IEEE 802.11bd-based V2X has been proposed. Still, it is unsuitable for ToD due to the short communication coverage [14], [15]. In contrast, C-V2X is more suitable for ToD operations because it is based on general cellular communication technologies such as 4G long-term evolution (LTE) and 5G new radio (NR). The inherent characteristics of cellular communications signify that they possess the appropriate coverage, connectivity, and data rate for ToD services. Therefore, C-V2X is primarily considered for the remote connections of ToD applications [9]. There are two interfaces defined by the 3rd Generation Partnership Project (3GPP) for V2X: the PC5 interface and the Uu interface, and both are applicable for providing real-time sensor sharing systems for ToD services [16]. The PC5 interface is based on sidelink communication, allowing direct connections without a base station (BS). It can be utilized for vehicle-to-vehicle (V2V), vehicle-to-infrastructure (V2I), and vehicle-to-pedestrian (V2P) communications, among others. By using the C-V2X PC5 interface, the vehicle can interact with a nearby roadside unit (RSU) and a tele-operation center for automated parking, for example [17]. On the other hand, Uu interface is based on uplink and downlink communications. It can provide remote network connectivity through a BS via vehicle-to-network (V2N) communication, which can facilitate connections between users or remote entities in different regions. Furthermore, since the uplink and downlink have broader bandwidth than the sidelink under the current situations, it can achieve higher data rates and support more users simultaneously.

However, only a limited number of literature related to C-V2X has considered high-volume data, such as camera sensor video, even though it is important for ToD applications. Moreover, previous works have focused on traditional factors for wireless communications, such as latency, data rate, and reliability. Consequently, the energy consumption of C-V2X has not yet been analyzed, despite the fact that the additional energy consumption for communications is significant for electric vehicles (EVs) due to battery constraints. The extra energy consumption implies a degradation of battery efficiency, which is critical to the performance of EVs. Therefore, it is essential to analyze the energy consumption involved in the communication process for sensor data transmissions to verify the impact of communication on battery efficiency. To address these demands, we analyzed the energy consumption associated with streaming camera sensor video data, which is the representative sensor data for ToD [11], under various conditions. The specific contributions are as follows:

- A new framework for analyzing energy consumption, which jointly reflects various channel conditions, data size, HARQ retransmissions, and bandwidth, is proposed based on link-level simulations. Utilizing the proposed framework, an analysis of the energy consumption in the vehicle resulting from the transmission of camera sensor video using 5G C-V2X was conducted, considering various video image resolutions.
- The tendency of energy consumption depending on signal-to-noise ratio (SNR) was analyzed considering various modulation and coding schemes (MCSs) and hybrid automatic repeat request (HARQ). The results indicate the effect of transport block size (TBS) and HARQ retransmissions due to communication errors on the total energy consumption of the C-V2X sensor sharing system.
- We considered multi-user scenarios and multi-camera sensor video transmissions, evaluating the increased energy consumption resulting from the utilization of

limited network resources and multi-user interference due to radio resource contention among multiple users.
- We investigated the energy consumption of sensor sharing systems in the vehicle for the ToD requirements. Also, we conducted a comparison with the use of an on-board unit (OBU). The results demonstrate how much energy can be saved for ToD compared to on-board processing of autonomous driving algorithms.

The rest of this paper is organized as follows. We begin with introducing the related work in section II. In Section III, the system model of energy consumption for C-V2X sensor sharing system is described. Section IV describes the configurations of the communication system, OBU, and EV for simulation. Section V describes the energy consumption simulation results. Finally, Section VI concludes the paper.

II. RELATED WORK

For real-time V2X applications, robust communication, low latency, and reliability are defined as key performance indicators (KPIs) by 3GPP and 5GAA for ITS [18], [19]. Therefore, previous literature has conducted research on communication performance of C-V2X based on the defined KPIs.

Representatively, researchers conducted latency analysis of the C-V2X system. Coll-Perales et al. proposed an end-to-end latency model for 5G V2N and vehicle-to-network-to-vehicle (V2N2V) communications, considering 800-byte packets, and analyzed it in light of latency requirements for various advanced V2X services [20]. The work done in [21] conducted the latency analysis of 5G V2N2V communication system, considering additional latency in control channels and retransmission latency due to k-repetitions and HARQ in shared channels. Choi et al. analyzed end-to-end latency and the elements of total latency for real-time sensor sharing system using 4G LTE and 5G NR C-V2X Uu interface, focusing on single camera video streaming [22]. Fouda et al. evaluated the C-V2X latency utilizing HARQ based on semi-persisten scheduling (SPS), taking into account vehicle density and bandwidth configurations [23]. Clancy et al. investigated the latency of handovers in 5G C-V2X Uu interface with consideration of quality-of-service (QoS) [24].

Also, there have been several studies considering reliability of C-V2X communications. Kim et al. analyzed the effect of denial-of-service (DoS) attacks on the reliability of LTE-based C-V2X sidelink [25]. Reyhanoglu et al. evaluated the reliability of C-V2X mode 4 concerning the packet size and MCS selection in terms of packet delivery ratio (PDR) [26]. The research done in [27] developed an enhanced and optimized media access control (MAC) protocol that can maintain high-reliability service. Li et al. proposed an AI-based roadside unit (RSU) planning method for C-V2X, considering the reliability while using data collected under real-world conditions [28]. The work done in [29] suggested a sensing sharing scheme to improve the reliability of C-V2X considering PDR for cooperative awareness messages (CAMs) and decentralized environmental notification message (DENM). Sunuwar et al. investigated the feasibility of 30 MHz bandwidth for C-V2X services requirements in terms of reliability and latency across varying vehicle density and quantities of RSUs [30].

Considering these traditional KPIs, various optimization frameworks have been proposed for resource allocation, latency minimization, and capacity enhancement. Cecchini et al. proposed a localization-based resource selection scheme for V2X sidelink [31]. The work done in [32] formulated an NP-hard resource allocation problem for dense C-V2X network and proposed a solution to enhance capacity leveraging the spatial reuse gain. Decarli et al. devised a V2X sidelink localization algorithm for low-latency and high-reliability networking required by platooning, which can also reduce sensor data overhead [33]. Bahonar et al. proposed a distributed framework for resource allocation considering V2V pairs [34]. Chen et al. suggests a reinforcement learning-based joint resource allocation and user scheduling method for latency minimization [35]. The work conducted in [36] security protocol for V2X handover which shows optimized latency while meeting the security requirements.

The traditional KPIs mentioned above are important factors in communication systems, and these existing studies have mainly focused on them to evaluate the communication performance of C-V2X. However, it is essential to be aware of the effect of energy consumption caused by the communication process, as there are battery constraints on EVs. The main contribution of this paper is to analyze the energy consumption associated with the transmission of sensor video data using the 5G C-V2X PC5 interface and Uu interface, which are required for ToD. We considered camera video as the sensor data to stream in real-time because it is a representative type of sensor for remote driving services. Also, we constructed the energy consumption model of C-V2X sensor sharing system and present simulation results that compare the energy consumption of ToD and OBU processing.

III. SYSTEM MODEL

In our model, we consider the scenarios in which a vehicle transmits sensor data for ToD using V2I and V2N, as shown in Fig. 1. For V2I, we assume that the vehicle transmits camera sensor video data to a nearby RSU using the 5G C-V2X PC5 interface. The RSU is directly connected to a nearby tele-operation center through sidelink, and the data received by the RSU are sent to the center. For V2N, we consider the 5G C-V2X Uu interface, which transmits data to a nearby BS and the BS sends the data to a remote entity, such as a remote user or cloud server, through the network. The control decisions of driving tasks are made by a tele-operation center or a remote entity, and control commands are transmitted back to the vehicle via C-V2X after the decisions for unmanned driving services are made. For comparison, we consider an unmanned vehicle processed

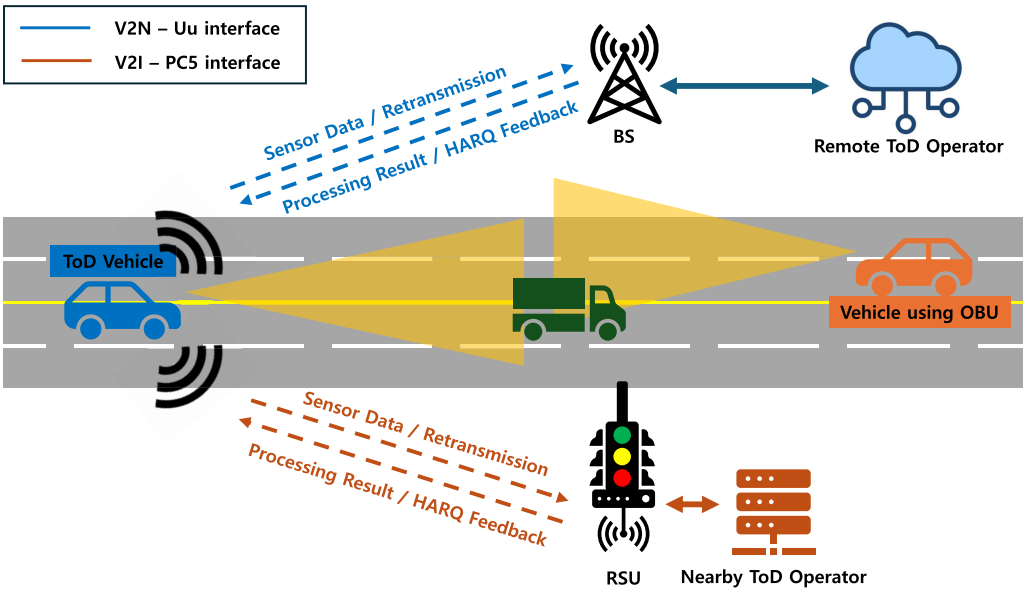

FIGURE 1. System model for driving operated by OBU and ToD, where ToD is facilitated via C-V2X sidelink or uplink.

by OBU. In this case, both recognition and control decision processes are entirely performed on the OBU unlike ToD-based vehicles.

Additionally, to ensure robust communication services, the vehicle can adjust the MCS based on the channel state. We assume the vehicle selects the MCS that minimizes end-to-end transmission latency and the time duration in active mode for ToD based on channel states, using the formula in [37] for simplicity. However, our model can be extended to consider various configurations and modifications that may affect the MCS. Additionally, we assume that the waveform for transmission passes through a fading channel, with zero-mean additive white Gaussian noise (AWGN) added to the waveform. In the event of an error, it is detected by the RSU or BS, as the receivers continuously check the cyclic redundancy check (CRC) bits of the received message for error detection. Furthermore, since we are considering HARQ, a negative acknowledgment (NACK) is transmitted to the vehicle if an error is detected in the received data bits, the vehicle is prompted to perform a retransmission. Under this scenario, we analyze the energy consumption of the vehicle for the transmission of sensor data.

To analyze the total energy consumption for communication of the vehicle, we consider an energy consumption model for the radio frequency (RF) transceiver in our analysis framework. The RF transceiver operates in two modes: active and inactive. When the RF transceiver is either transmitting or receiving the radio signal, all its functional blocks are active, thereby defining the active mode. Otherwise, when the RF transceiver is in an idle state, without transmitting or receiving any radio signal, it is considered to be in inactive mode. To assess the impact of energy consumption on vehicle performance, we define the networking energy as the total energy consumed by the RF transceiver to transmit a video frame using V2X, denoted as E_{V2X}, which is expressed as

$$E_{V2X} = E_{sleep} + E_{on} + E_{trans}, \tag{1}$$

where E_{sleep} represents the energy consumption when the RF transceiver is in inactive mode, E_{on} represents the energy consumed during signal transmission, and E_{trans} is the energy consumption when the transceiver is in transient mode [38]. The energy consumption in transient mode occurs when transitioning between active mode and inactive mode due to the inherent properties of transceiver blocks, which can cause non-ideality, including local oscillator (LO) start-up current, inrush current, amplifier settling time, and phase-locked loop (PLL) delay. It is decided as

$$E_{trans} = P_{trans} T_{trans}, \tag{2}$$

where P_{trans} is the power consumption in transient mode, and T_{trans} is the time duration of transient mode. Meanwhile, E_{sleep} can be determined as

$$E_{sleep} = P_{sleep} T_{sleep}, \tag{3}$$

where P_{sleep} and T_{sleep} are the power level and time duration of the inactive state of the RF transceiver, respectively. Similarly, E_{on} is determined as

$$E_{on} = P_{on} T_{on}, \tag{4}$$

where P_{on} is the power level when the transceiver is active and T_{on} is the time duration of the active state of the transmitter. The other elements of the energy consumption model are described in detail as follows.

- The active time duration, T_{on}, is defined as

$$T_{on} = T_{tx} + T_{retrans}, \tag{5}$$

where T_{tx} is the time duration of initial transmission and $T_{retrans}$ is the time for HARQ retransmission [20].

When the bit size of the video frame exceeds the transport block size (TBS), it cannot be sent in a single transmission time interval (TTI) unit. Therefore, the data are transmitted over several TTI units through segmentation. Therefore, T_{tx} can be calculated as

$$T_{tx} = \lceil \frac{N_{video}}{N_{TBS}} \rceil \times t_{TTI}, \tag{6}$$

where $\lceil \cdot \rceil$ is the ceiling function, N_{video} is the bit size of each video frame, N_{TBS} is the bit size of TBS, and t_{TTI} is the TTI duration. N_{video} is determined as

$$N_{video} = \frac{HWD}{C_r}, \tag{7}$$

where H and W are the height and width of the camera video frame in the number of pixels, D is the color depth, and C_r is the data compression ratio. C_r can be decided as follows,

$$C_r = \frac{N_{video,Raw}}{N_{video,Comp}}, \tag{8}$$

where $N_{video,Raw}$ is the bit size of raw video before compression with encoding, and $N_{video,Comp}$ is the bit size of compressed video after encoding. N_{TBS} is affected by the modulation order and code rate, and the detailed process for calculation of N_{TBS} is presented in [39]. If the code rate is less than 1/4, it can be calculated as

$$N_{TBS} = 8C\lceil \frac{N'_{info} + 24}{8C} \rceil - 24, \tag{9}$$

where $C = \lceil (N'_{info} + 24)/3816 \rceil$. Otherwise, it can be determined as

$$N_{TBS} = \begin{cases} 8C\lceil \frac{N'_{info} + 24}{8C} \rceil - 24, & \text{if } N'_{info} > 8424, \\ 8\lceil \frac{N'_{info} + 24}{8} \rceil - 24, & \text{otherwise}, \end{cases} \tag{10}$$

where $C = \lceil (N'_{info} + 24)/8424 \rceil$. N'_{info} is the quantized intermediate number of information bits, which is defined as

$$N'_{info} = \max\left(3840, 2^n \text{round}\left(\frac{N_{info} - 24}{2^n}\right)\right), \tag{11}$$

where round $(\cdot)$ is the round function, and $n = \lfloor \log_2 (N_{info} - 24) \rfloor - 5$ where $\lfloor \cdot \rfloor$ is the floor function. N_{info} is the unquantized intermediate variable, which is presented as

$$N_{info} = N_{RE} R Q_m, \tag{12}$$

where N_{RE} is the number of allocated resource elements (REs) within the slot, R is the code rate, and Q_m is the modulation order. N_{RE} is obtained as

$$N_{RE} = \min(156, N'_{RE}) n_{PRB}, \tag{13}$$

where n_{PRB} is the number of allocated physical resource blocks (PRBs) for a vehicle, and N'_{RE} is the number of REs allocated within a PRB. N'_{RE} is determined as

$$N'_{RE} = N_{sc}^{RB} N_{symbol}^{sh} - N_{DMRS}^{PRB} - N_{oh}^{PRB}, \tag{14}$$

where N_{sc}^{RB} is the number of subcarriers in a PRB, N_{symbol}^{sh} is the number of symbols within the slot, N_{DMRS}^{PRB} is the number of REs for dedicated demodulation reference signals (DM-RS) per PRB, and N_{oh}^{PRB} is the overhead decided by higher layer parameters.

- If the receiver sends NACK to the vehicle after detecting error, the vehicle must send the data again, and this retransmission occurs with extra time of active mode for communication. The retransmission time duration, $T_{retrans}$, can be derived as

$$T_{retrans} = n_{retrans} t_{TTI}, \tag{15}$$

where $n_{retrans}$ is the number of retransmissions since each retransmission uses 1 TTI duration.

- The power level of the RF transceiver in active mode, P_{on}, is defined as

$$P_{on} = P_{PA} + P_{others}, \tag{16}$$

where P_{PA} is the power consumed by the power amplifier (PA) and P_{others} is the power consumed by other blocks of the RF transceiver, which is illustrated in Fig. 2. The power consumed by the PA is presented as

$$P_{PA} = P_t/\delta, \tag{17}$$

where P_t is the power of signal at the digital baseband and δ is the PA efficiency. P_{others} is a combination of power consumed by a digital-to-analog converter (DAC), an analog-to-digital converter (ADC), filters, LOs, mixers, a low-noise amplifier (LNA), etc. Therefore, it can be determined as

$$P_{others} = P_{DAC} + P_{etc}, \tag{18}$$

where P_{DAC} is the power consumed by DAC, and P_{etc} is the power level consumed by other blocks of the RF transceiver [38].[1] To summarize, E_{on} is derived as

$$E_{on} = T_{on}(P_t/\delta + P_{DAC} + P_{etc}). \tag{19}$$

To compare E_{V2X} with the energy consumption of the OBU, we consider an on-board CPU as the computation unit within the vehicle. To calculate the energy used by CPU for recognition and control decision task, we utilize the energy consumption model of CPU, E_{CPU}, as follows,

$$E_{CPU} = P_{CPU} t_e, \tag{20}$$

where t_e is the execution time duration. P_{CPU} is the power consumption of CPU, which can be presented as,

$$P_{CPU} = k_1 f^3 + k_0, \tag{21}$$

[1]Since we consider the uplink sensor sharing system and sidelink transmitting system, the power consumed by receiving is fixed for simplicity. However, it can be easily extended by slightly modifying the formula.

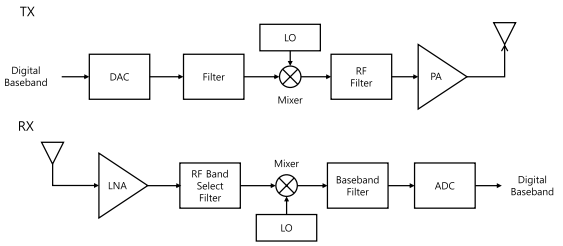

FIGURE 2. Block diagram of in-vehicle RF transceiver circuit for 5G C-V2X.

TABLE 1. MCS indices and spectral efficiency for NR Sidelink.

MCS index	Modulation order	Code rate	Spectral efficiency
7	2	0.5137	1.0273
13	4	0.4785	1.9141
19	6	0.5049	3.0293
27	6	0.8887	5.3320

TABLE 2. MCS indices and spectral efficiency for NR uplink.

MCS index	Modulation order	Code rate	Spectral efficiency
4	2	0.5879	1.1758
10	4	0.6426	2.5703
19	6	0.8525	5.1152
27	8	0.9258	7.4063

where k_1 and k_2 are the coefficients decided by CPU architecture, f is the on-board CPU frequency [40], [41].

IV. SIMULATION CONFIGURATION

In this section, we describe the simulation configuration used to analyze the energy consumption by the 5G C-V2X real-time sensor sharing system. We examine the energy consumption incurred during sensor sharing, taking into account two interfaces: the 5G C-V2X sidelink and uplink. The vehicle transmits camera video for sensor sharing to a nearby RSU and BS. The detailed descriptions of the configurations are as follows.

A. CONFIGURATIONS OF COMMUNICATION SYSTEM

We assume that the bandwidth is 20 MHz and 100 MHz for the sidelink, which utilizes time-division duplexing (TDD), and 100 MHz for the uplink, which employs frequency-division duplexing (FDD) [42]. The subcarrier spacing (SCS) and TTI are fixed to 60 kHz and 0.25 ms, respectively. In addition, it is assumed that the total bandwidth is fully utilized for the sensor sharing system. For multi-user access, we assume that the bandwidth is fairly allocated in an orthogonal manner based on PRBs. In uplink scenarios, we assume that scheduling is managed by the BS using the method defined in [43]. Furthermore, we assume that the sidelink operates based on 5G C-V2X mode 2, which schedules resources by sensing-based semi-persistent scheduling (SB-SPS) based on autonomous resource selection [44].

The power consumed by the PA is set to 23 dBm (approximately 200 mW), which is the standard power level for C-V2X transmitters [45]. In addition, the power

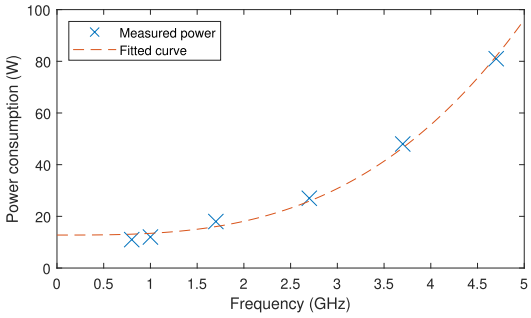

FIGURE 3. The empirical power consumption data of CPU based on its frequency and the fitted function which is matched with the CPU energy consumption model.

consumption of the circuits for the RF transceiver follows the values in [38] and [46]. For channel coding, low-density parity check (LDPC) coding is employed, while quadrature phase shift keying (QPSK) and quadrature amplitude modulation (QAM) are utilized as the modulation schemes, both of which are commonly used in 5G communication systems [47], [48], [49]. Additionally, MCS indices from Tables 5.1.3.1-1 and 5.1.3.1-2 in [39], as defined by the 3GPP for 5G C-V2X, were utilized for the simulations of sidelink and uplink, respectively. The MCS indices for the simulation were selected based on modulation order and spectral efficiency, with their detailed parameters organized in Table 1 and Table 2.

For HARQ, we consider chase combining (CC)-HARQ, as it is generally regarded as more appropriate than incremental redundancy (IR)-HARQ due to its simpler implementation and lower latency [50], [51], [52]. In CC-HARQ, the same messages are transmitted for each retransmission round. Typically, there is a maximum number of retransmission rounds for HARQ to prevent network congestion [52]. Therefore, in this simulation, transmission is considered a failure if an error is detected during the third retransmission. Also, we assume that NACK messages in the HARQ process are always sent without error for brevity.

For the fading channel, we consider a Rayleigh fading channel, which is typically used statistical model for wireless communication circumstances without line-of-sight (LOS) between the transceivers. The model used in this simulation for the Rayleigh fading channel is the clustered delay line (CDL) channel, as defined by the 3GPP standard and widely used for link-level simulations of 5G NR communication systems [53]. For the detailed channel configuration, we utilized the V2X channel for the urban highway environment as modeled by 3GPP [54]. For the simulations, the transceiver and fading channel models were built using the 5G Toolbox and Communications Toolbox in MATLAB R2022b [55], [56].

B. OTHER CONFIGURATIONS

1) SENSOR VIDEO SHARING SYSTEM

We assume that the vehicle can choose the resolution of the video to be transmitted, depending on channel states

TABLE 3. Parameter configuration for simulation.

Parameters	Sidelink (PC5)	Uplink (Uu)
Bandwidth	20, 100 MHz	100 MHz
MCS index	7, 13, 19, 27	4, 10, 19, 27
Subcarrier spacing	60 kHz	
TTI duration	0.25 ms	
PA power	200 mW	
DAC power	17.8 mW	
Transceiver power of other blocks	305.8 mW	
Transient mode power	125 mW	
Inactive mode power	50 mW	
Channel model	CDL channel	
Channel coding	LDPC code	
Noise figure	6 dB	
Video resolution	HD, FHD, QHD, UHD, 8K	
Color depth of video	24 bits	
Encoding format	H.264 AVC	
Encoding level	6	
Idle state CPU frequency	800 MHz	
Base CPU frequency	3.7 GHz	
Maximum CPU frequency	4.7 GHz	

and user requirements. We consider high definition (HD), full HD (FHD), quad HD (QHD), ultra HD (UHD), and 8K UHD (8K) for the resolutions of camera video. The sizes in pixels for these five resolutions are 1280 by 720 for HD, 1920 by 1080 for FHD, 2560 by 1440 for QHD, 3480 by 2160 for UHD, and 8192 by 4320 for 8K. The video data are compressed with a fixed encoding format, H.264 Advanced Video Coding (AVC), which is a widely used standard for moving video encoding and considered as reference encoding format for ToD by 5GAA [11], [57], [58], [59]. H.264 AVC provides superior compression efficiency with manageable processing complexity compared to its successors, H.265, H.266 and AOMedia Video 1 (AV1), which offer marginal performance gains at the expense of substantially increased algorithmic complexity [60]. Also, the encoding level is fixed at 6, and the traffic size of the compressed video frame, $N_{video,Comp}$, adheres to the maximum data traffic specified in [58] for simplicity. Besides, the color depth of the camera sensor video frame is assumed to be 24 bits, and the frame rate of the video is set at 30 frames per second (fps), which are necessary for ToD requirements [61], [62].

2) CPU MODEL

We also analyze the difference in energy efficiency between the sensor sharing system for ToD and on-board CPUs. For configurations of on-board CPU, we utilized the empirical power consumption data of the Intel i7-8700K CPU model. The power consumption data were measured for various CPU frequencies using the overclock checking tool (OCCT). Based on the measured power consumption at six CPU frequencies, we created a fitted function for the measured data which is matched with (21), as shown in Fig. 3. Therefore, the coefficients of the fitted curve, k_1 and k_0, are approximately 6.668×10^{-28} W/Hz^3 and 12.7652 W, respectively. Also, in the idle state of the CPU, the clock frequency, f_{idle}, was measured to be 800 MHz. According to the specification sheet of the CPU, its base clock frequency, f_{base}, is 3.7 GHz,

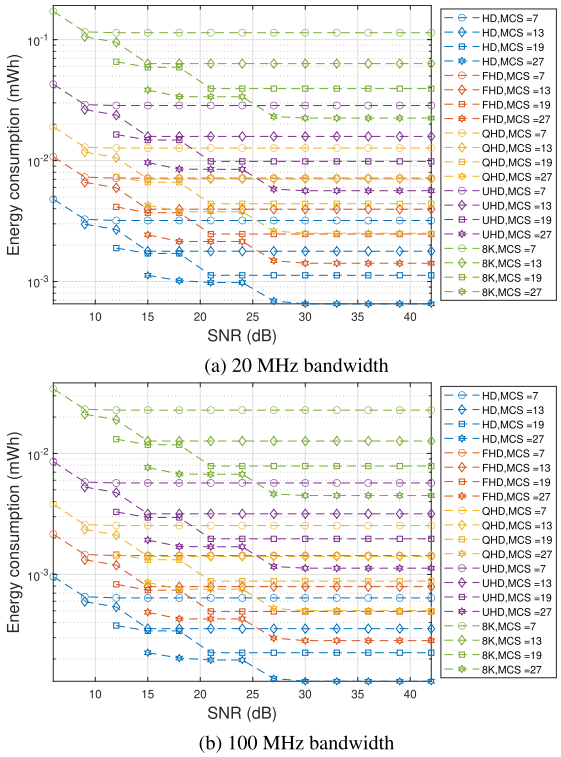

(a) 20 MHz bandwidth

(b) 100 MHz bandwidth

FIGURE 4. The energy consumption per frame for a single user using the C-V2X sidelink, depending on various SNR values.

and it can speed up to its max frequency, f_{max}, which is 4.7 GHz [63].

The remaining parameters applied to the simulations are organized in Table 3.

V. SIMULATION RESULTS AND ANALYSIS

In this section, we analyze the total energy consumption for camera sensor video data transmission based on the 5G C-V2X communication system. Also, we conduct a comparison between the energy consumption of sensor sharing for ToD and that of the OBU.

A. SIDELINK SENSOR SHARING SYSTEM

First, we analyze E_{V2X} consumed for sensor sharing using the 5G C-V2X sidelink to a nearby RSU. Fig. 4 shows the energy consumption for sending a single camera sensor data frame, depending on various SNR values and video resolutions when a single user transmits the sensor data to an RSU. Lower SNR values result in higher energy consumption because increased path loss leads to more communication errors and additional retransmissions. Also, selecting a lower MCS index increases energy consumption by reducing the TBS and prolonging T_{tx}, while higher MCS indices, though faster, are more vulnerable to errors, leading to more retransmissions. To compare the results in terms of bandwidth, the same approach can be applied. When the bandwidth is 20 MHz, as shown in Fig. 4, the energy consumption is relatively large compared to the results in Fig. 4b due to the smaller TBS, which results from the narrower bandwidth. Meanwhile, higher video resolutions

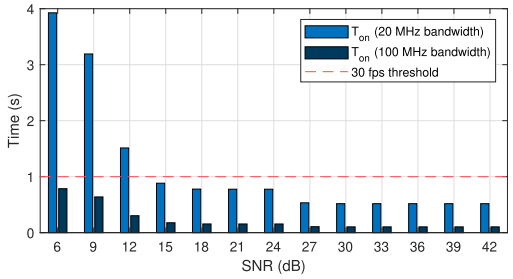

(a) The required time duration of active mode depending on SNR, when the vehicle transmits 30 frames of 4 HD videos and utilizes MCS that makes T_{on} minimum.

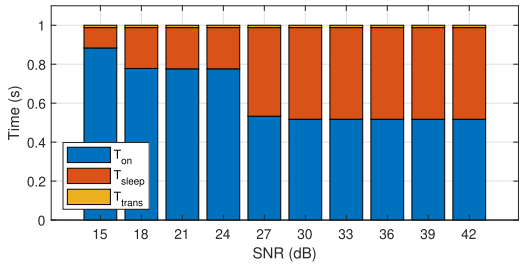

(b) T_{on}, T_{sleep}, and T_{trans} when the vehicle transmits videos without timeout for one second and the bandwidth is 20 MHz.

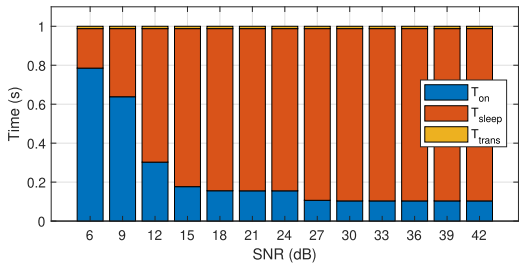

(c) T_{on}, T_{sleep}, and T_{trans} when the vehicle transmits videos without timeout for one second and the bandwidth is 100 MHz.

FIGURE 5. T_{on}, T_{sleep} and T_{trans} when a single user is transmitting 4 HD camera videos at 30 fps using C-V2X PC5 interface.

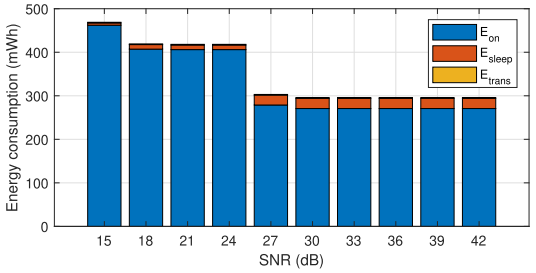

(a) 20 MHz bandwidth

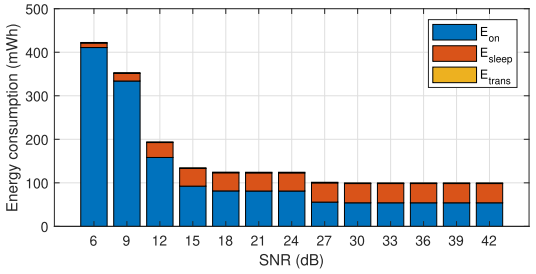

(b) 100 MHz bandwidth

FIGURE 6. E_{on}, E_{sleep}, and E_{trans} depending on SNR when a single user is transmitting 4 HD camera videos at 30 fps using C-V2X PC5 interface.

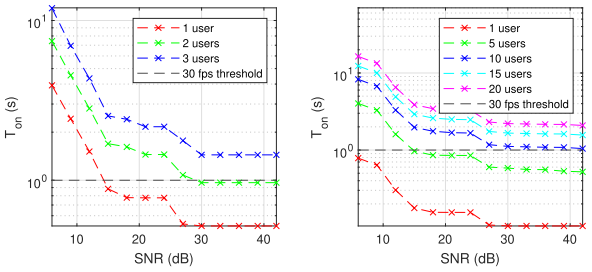

(a) T_{on}, 20 MHz bandwidth

(b) T_{on}, 100 MHz bandwidth

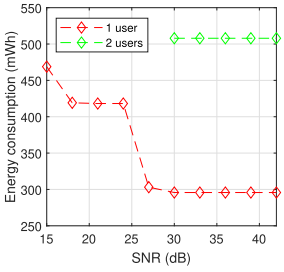

(c) E_{V2X}, 20 MHz bandwidth

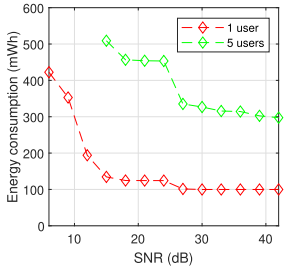

(d) E_{V2X}, 100 MHz bandwidth

FIGURE 7. T_{on} and E_{V2X} when multiple single users are sharing the bandwidth and the user is transmitting 4 HD camera videos at 30 fps using C-V2X PC5 interface.

increase energy consumption due to the larger bit size of the video frames, which implies longer T_{on}.

To evaluate the energy consumption of ToD, we investigated the energy used for one hour when the vehicle is transmitting four camera videos simultaneously at 30 fps [9]. Fig. 5a presents T_{on} depending on SNR when the user transmits 30 frames of four HD videos. At lower SNR levels, video transmission requires more time, thus T_{on} also becomes longer. When the bandwidth is 20 MHz and SNR falls below 15 dB, the transmission time for four videos at 30 frames exceeds one second, leading to a timeout. In contrast, no timeout occurs when the bandwidth is 100 MHz, as the larger bandwidth reduces T_{on}. Fig. 5b and Fig. 5c illustrate T_{on}, T_{sleep}, and T_{trans} as a function of SNR when the user transmits 30 frames of four HD videos without timeout. When T_{on} is longer, then T_{sleep} becomes shorter because T_{sleep} is the remaining time after the video transmission. On the other hand, T_{trans} remains nearly constant, as it depends not on SNR but on the number of transitions and inherent non-ideality of RF transceiver. Fig. 6 illustrates the energy consumption when the user transmits four HD videos at 30 fps to a nearby RSU over one hour. Since P_{on} is greater than P_{sleep}, a longer T_{on} results in higher energy consumption. In terms of bandwidth, energy consumption is higher at 20 MHz than at 100 MHz due to the impact of bandwidth on TBS. Meanwhile, E_{trans} appears almost negligible because T_{trans} is extremely short compared to T_{on} and T_{sleep}, even though P_{trans} is not insignificant.

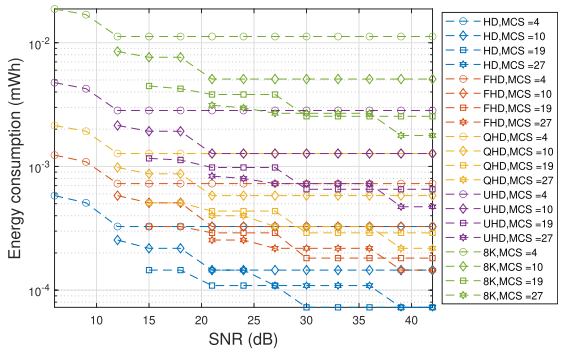

FIGURE 8. The energy consumption per frame for a single user using the C-V2X uplink, depending on various SNR values.

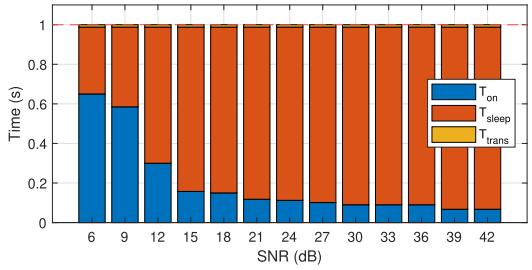

FIGURE 9. T_{on}, T_{sleep}, and T_{trans} when a single user is transmitting 4 HD camera videos at 30 fps using C-V2X Uu interface and utilizing MCS that makes T_{on} minimum.

Fig. 7a and Fig. 7b present T_{on} as a function of SNR when multiple users share the fixed 20 MHz and 100 MHz bandwidth for 5G V2X sidelink, and the user is transmitting four HD videos at 30 fps and utilizing MCS which makes the T_{on} minimum. If the SNR is lower than 30 dB and the bandwidth is 20 MHz, ToD cannot be supported when multiple users are occupying the network due to the occurrence of timeout. Fig. 7c and Fig. 7d illustrate the minimum energy consumption for ToD as a function of SNR when multiple users share the fixed 20 MHz and 100 MHz bandwidth, and the user is transmitting four HD videos at 30 fps. As the number of users sharing the bandwidth increases, the total energy consumption for a single user also increases. This is due to the fact that sharing bandwidth with more users makes TBS smaller, and a smaller TBS results in a longer T_{on}. Additionally, resource allocation for sidelink mode 2 is based on autonomous scheduling method for multiple users [44]. This results in increased contention for radio resource among users and additional interference, which may lead to a higher error rate and more frequent retransmissions.

B. UPLINK SENSOR SHARING SYSTEM

Following a similar approach as in the subsection V-A, we investigate E_{V2X} consumed for sensor data transmission using the C-V2X uplink to an adjacent BS. Fig. 8 shows the energy consumption required to transmit a single frame of camera sensor video, depending on the SNR and video resolutions, when a single user sends sensor data to the BS. The trend in energy consumption across SNR, MCS, and resolution is consistent with the result observed for the

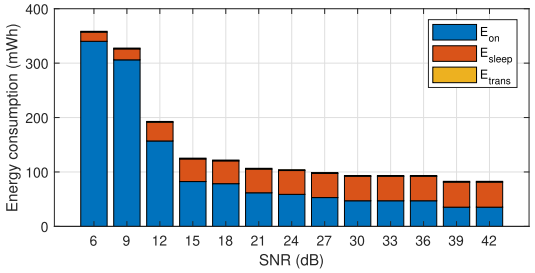

FIGURE 10. E_{on}, E_{sleep}, and E_{trans} depending on SNR when a single user is transmitting 4 HD camera videos at 30 fps using C-V2X Uu interface.

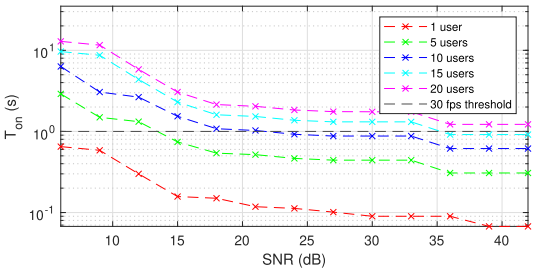

(a) T_{on} depending on the number of users sharing the bandwidth, when the user transmits video at 30 fps for one second and utilizes MCS that makes T_{on} minimum.

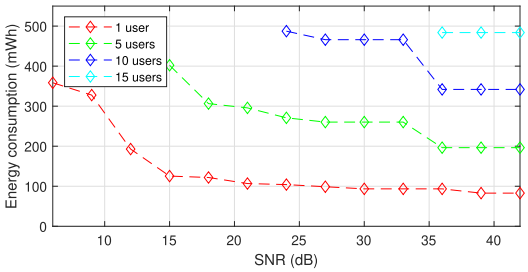

(b) E_{V2X} depending on the number of users sharing the bandwidth, when the user transmits video at 30 fps for an hour.

FIGURE 11. T_{on} and E_{V2X} as a function of SNR when multiple single users are sharing the bandwidth and the user is transmitting 4 HD camera videos at 30 fps using C-V2X Uu interface.

sidelink which is presented in Fig. 4. However, the overall energy consumption is significantly lower compared to using the C-V2X sidelink. It is because the C-V2X uplink utilizes higher spectral efficiency due to the use of different MCS, resulting in larger TBS and reduced T_{on}.

Fig. 9 illustrates T_{on} and T_{sleep} by SNR when the vehicle transmits 30 frames of four HD videos. The tendency is similar to Fig. 5a, but T_{on} is shorter due to the larger TBS, resulting in longer T_{sleep} and no timeout. Fig. 10 shows the energy consumption when the user transmits four HD videos at 30 fps over an hour to an adjacent BS. Similarly, the trend of energy consumption by SNR is similar to Fig. 6, but the energy consumption is significantly lower compared to the C-V2X sidelink because of the same reasons mentioned above.

Fig. 11a presents T_{on} as a function of SNR when multiple users share 100 MHz bandwidth, and the user is streaming four HD video at 30 fps. The results show that ToD is available through 5G C-V2X uplink when up to 15 users are sharing the bandwidth. Excluding the cases where the

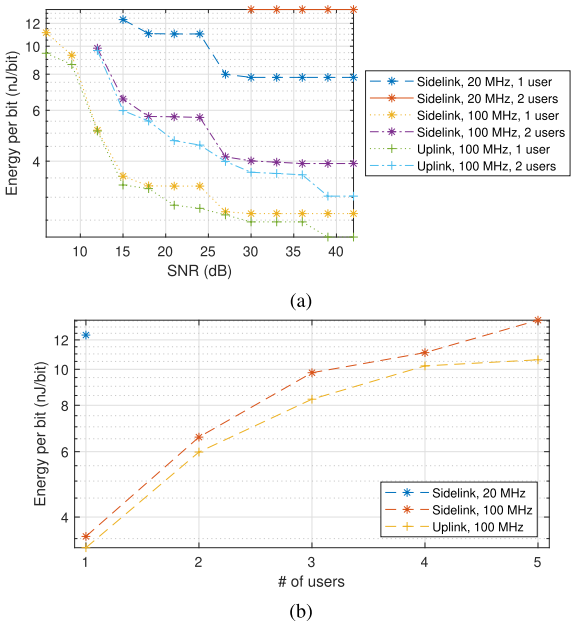

FIGURE 12. (a) Energy per bit depending on SNR when the number of vehicles sharing the bandwidth is 1 or 2. (b) Energy per bit depending on the number of vehicles sharing the bandwidth when the SNR is 15 dB.

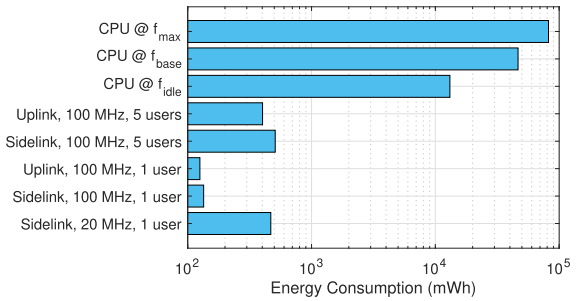

FIGURE 13. Energy consumption comparison between ToD and OBU. The vehicle transmits 4 HD videos at 30 fps over one hour for ToD and the SNR is 15 dB and the operating frequency of the CPU remains constant for one hour.

timeout occurs, as shown in Fig. 11b, the energy consumption increases as the SNR decreases or the number of users sharing the bandwidth rises, while the amount of increase remains lower than that of the sidelink, even with a larger number of users. This also can be attributed to the utilization of a larger bandwidth and different MCS indices. A larger bandwidth leads to more PRBs available in the bandwidth, which allows each user to access more PRBs and a larger TBS per user. Also, it is influenced by the use of different MCS, which results in a larger TBS. These two factors consequently shorten T_{tx}, and shorter T_{tx} means smaller T_{on}, leading to smaller E_{on}. Similar to the results presented in Fig. 7c and Fig. 7d, contention among multiple vehicles leads to additional retransmissions and increased energy consumption. However, the magnitude of this increase is lower than that observed in sidelink communication. This difference arises because uplink scheduling is centrally managed by BS, thereby reducing the frequency of contention among vehicles compared to sidelink communication, which relies on autonomous resource selection [44].

Fig. 12 presents a comparison of energy per bit between sidelink and uplink. In Fig. 12a, energy per bit is shown as a function of SNR. When comparing sidelink cases, operating with a 100 MHz bandwidth consumes, on average, approximately 27% of the energy required for a 20 MHz bandwidth at a given SNR, primarily due to the shorter T_{on}. Also, when comparing sidelink and uplink under the same bandwidth conditions, uplink-based sensor sharing consumes approximately 85% of the energy consumed for sidelink. It is due to the TBS and the prevalence of contention, which arises from differences in scheduling properties. In Fig. 12b, energy per bit depending on the number of users is illustrated. Ideally, the same amount of PRB is allocated per vehicle in sidelink when a single user operates with a 20 MHz bandwidth and when five users share a 100 MHz bandwidth. However, resource sharing among multiple users entails contention, which in turn increases energy consumption. The results indicate that uplink outperforms sidelink at energy efficiency due to the use of different MCS. Additionally, uplink exhibits superior performance in dense radio traffic conditions due to the BS-based scheduling mechanism.

Fig. 13 presents the energy consumption in the vehicle when the driving is managed by OBU, ToD using C-V2X sidelink, and ToD using uplink over one hour and the SNR is 15 dB. The OBU consumes 46.54 Wh and 81.99 Wh when it is being operated at f_{base} and f_{max}, respectively. In contrast, using ToD consumes less than 0.51 Wh. These indicate that employing ToD can save 100∼650 times more energy compared to using OBU. Moreover, OBU consumes 13.11 Wh for one hour when its operating frequency is f_{idle}, which means the energy consumption of ToD is at least 25 times more energy-efficient even if the OBU is in the idle state. In a comparison between sidelink and uplink, sidelink consumes 1.1∼3.7 times larger power than the uplink when a single user utilizes the bandwidth. Also, even when five users share the bandwidth of 100 MHz using uplink, it consumes less energy than when a single user dominates the total bandwidth of 20 MHz for sidelink.

VI. CONCLUSION

In this paper, we proposed a framework for analysis of energy consumption considering various environmental conditions of wireless communications, and we analyzed the energy consumption resulting from sensor sharing for ToD using 5G C-V2X based on the proposed framework. Our analysis considered various video resolutions under different conditions, including varying channel states and multi-user scenarios. The increase in energy consumption can be attributed to a smaller TBS resulting from lower MCS indices or bandwidth sharing, both of which compel the vehicle to consume more energy for initial transmissions by making the duration of active mode longer. Higher video resolutions can further increase energy consumption, as larger data sizes necessitate more TTIs for transmission. In addition, SNR significantly affects total energy consumption. With lower SNR, more communication errors occur, leading to an

increased number of retransmission trials, which results in a longer time duration of active mode for RF transceiver and higher energy consumption. Multi-user contention for radio resources can also increase energy consumption by inducing additional retransmissions due to interference. Additionally, the results demonstrate that using the uplink is more energy efficient than using the sidelink, owing to the differences in TBS and scheduling properties. Compared to the energy consumption of the on-board CPU, ToD showed higher energy efficiency. This suggests that ToD is more effective than autonomous driving systems operated by the OBU in reducing additional energy consumption of vehicles required to support unmanned mobility services. For future work, we will consider variable transmission power and derive an energy consumption optimization model under variable channel conditions and traffic density considering scheduling methods and security aspects for the C-V2X-based real-time sensor sharing system.

REFERENCES

[1] *Taxonomy and Definitions for Terms Related To Driving Automation Systems for On-Road Motor Vehicles*, SAE Standard J3016, 2021.

[2] S. Oh, R. Seshadri, D.-T. Le, P. C. Zegras, and M. E. Ben-Akiva, "Evaluating automated demand responsive transit using microsimulation," *IEEE Access*, vol. 8, pp. 82551–82561, 2020.

[3] S. Zhang, C. Markos, and J. J. Q. Yu, "Autonomous vehicle intelligent system: Joint ride-sharing and parcel delivery strategy," *IEEE Trans. Intell. Transp. Syst.*, vol. 23, no. 10, pp. 18466–18477, Oct. 2022.

[4] J. Diechmann, E. Ebel, K. Heineke, R. Heuss, M. Kellner, and F. Steiner. *Autonomous Driving's Future: Convenient and Connected*. Accessed: Feb. 13, 2025. [Online]. Available: https://www.mckinsey.com/industries/automotive-and-assembly/our-insights/autonomous-drivings-future-convenient-and-connected

[5] R. Curry. *2 Waymo Self-driving Cars Stall At SF Pride Parade Street Closures During Heavy Traffic*. Accessed: Feb. 13, 2025. [Online]. Available: https://abc7news.com/waymo-stalled-self-driving-car-sf-pride-robotaxi/13427435/

[6] M. L. Cummings. *What Self-Driving Cars Tell Us About AI Risks: 5 Conclusions From an Automation Expert Fresh Off a Stint With the U.S. Highway Safety Agency*. IEEE Spectr. Accessed: Feb. 13, 2025. [Online]. Available: https://spectrum.ieee.org/self-driving-cars-2662494269

[7] Y. Lu. *Lost Time for No Reason: How Driverless Taxis Are Stressing Cities*. New York Times. Accessed: Feb. 13, 2025. [Online]. Available: https://www.nytimes.com/2023/11/20/technology/driverless-taxis-cars-cities.html

[8] E. Güney, C. Bayilmis, and B. Çakan, "An implementation of real-time traffic signs and road objects detection based on mobile GPU platforms," *IEEE Access*, vol. 10, pp. 86191–86203, 2022.

[9] *C-V2X Use Cases Volume II: Examples and Service Level Requirements*, 5GAA, Berlin, Germany, 2020.

[10] O. Amador, M. Aramrattana, and A. Vinel, "A survey on remote operation of road vehicles," *IEEE Access*, vol. 10, pp. 130135–130154, 2022.

[11] *Tele-operated Driving Use Cases, System Architecture and Bus. Considerations*, 5GAA, Berlin, Germany, 2021.

[12] R. Molina-Masegosa, J. Gozalvez, and M. Sepulcre, "Comparison of IEEE 802.11p and LTE-V2X: An evaluation with periodic and aperiodic messages of constant and variable size," *IEEE Access*, vol. 8, pp. 121526–121548, 2020.

[13] T. V. Nguyen, P. Shailesh, B. Sudhir, G. Kapil, L. Jiang, Z. Wu, D. Malladi, and J. Li, "A comparison of cellular vehicle-to-everything and dedicated short range communication," in *Proc. IEEE Veh. Netw. Conf. (VNC)*, Nov. 2017, pp. 101–108.

[14] G. Naik, B. Choudhury, and J.-M. Park, "IEEE 802.11bd & 5G NR V2X: Evolution of radio access technologies for V2X communications," *IEEE Access*, vol. 7, pp. 70169–70184, 2019.

[15] S. O. Oladejo and O. E. Falowo, "Latency-aware dynamic resource allocation scheme for multi-tier 5G network: A network slicing-multitenancy scenario," *IEEE Access*, vol. 8, pp. 74834–74852, 2020.

[16] *Architecture Enhancements for V2X Services*, document TS 23.285, Version 18.0.0, 3GPP, 2024.

[17] N. Ambrosy, J. Rainer, M. Niebisch, R. German, and L. Underberg, "Self-navigating automotive production: Using 5G for automated driving in car assembly," in *Proc. IEEE 18th Int. Conf. Factory Commun. Syst. (WFCS)*, Apr. 2022, pp. 1–4.

[18] *Service Requirements for Enhanced V2X Scenarios*, document TS 22.186, Version 18.0.1, 3GPP, 2024.

[19] *5G-V2X Direct Communication Evaluation Approach: An Automotive*, 5GAA, Berlin, Germany, 2024.

[20] B. Coll-Perales, M. C. Lucas-Estañ, T. Shimizu, J. Gozalvez, T. Higuchi, S. Avedisov, O. Altintas, and M. Sepulcre, "End-to-end V2X latency modeling and analysis in 5G networks," *IEEE Trans. Veh. Technol.*, vol. 72, no. 4, pp. 5094–5109, Apr. 2023.

[21] M. C. Lucas-Estañ, B. Coll-Perales, T. Shimizu, J. Gozalvez, T. Higuchi, S. Avedisov, O. Altintas, and M. Sepulcre, "An analytical latency model and evaluation of the capacity of 5G NR to support V2X services using V2N2 V communications," *IEEE Trans. Veh. Technol.*, vol. 72, no. 2, pp. 2293–2306, Feb. 2023.

[22] S. Choi, D. Kwon, and J.-W. Choi, "Latency analysis for real-time sensor sharing using 4G/5G C-V2X uu interfaces," *IEEE Access*, vol. 11, pp. 35197–35206, 2023.

[23] A. Fouda, R. Berry, and I. Vukovic, "HARQ retransmissions in C-V2X: A BSM latency analysis," in *Proc. ICC - IEEE Int. Conf. Commun.*, Jun. 2024, pp. 4317–4322.

[24] J. Clancy, D. Mullins, E. Ward, P. Denny, E. Jones, M. Glavin, and B. Deegan, "Investigating the effect of handover on latency in early 5G NR deployments for C-V2X network planning," *IEEE Access*, vol. 11, pp. 129124–129143, 2023.

[25] K. Kim, D. Kwon, W.-C. Jin, S. Choi, J. Kim, and J.-W. Choi, "Fatal C-V2X denial-of-service attack degrading quality of service in a highway scenario," *J. Commun. Netw.*, vol. 26, no. 2, pp. 182–192, Apr. 2024.

[26] A. Reyhanoglu, E. Kar, F. E. Kumec, Y. S. Can Kara, S. Karaagac, B. Turan, and S. Coleri, "On the reliability analysis of C-V2X mode 4 for next generation connected vehicle applications," in *Proc. IEEE 96th Veh. Technol. Conf. (VTC-Fall)*, Sep. 2022, pp. 1–5.

[27] X. Gu, J. Peng, L. Cai, Y. Cheng, X. Zhang, W. Liu, and Z. Huang, "Performance analysis and optimization for semi-persistent scheduling in C-V2X," *IEEE Trans. Veh. Technol.*, vol. 72, no. 4, pp. 4628–4642, Apr. 2023.

[28] P. Li, K. Wu, Y. Cheng, S. T. Parker, and D. A. Noyce, "How does C-V2X perform in urban environments? Results from real-world experiments on urban arterials," *IEEE Trans. Intell. Vehicles*, vol. 9, no. 1, pp. 2520–2530, Jan. 2024.

[29] S. Ha, W. Yoo, H. Kim, and J.-M. Chung, "C-V2X adaptive short-term sensing scheme for enhanced DENM and CAM communication," *IEEE Wireless Commun. Lett.*, vol. 11, no. 3, pp. 593–597, Mar. 2022.

[30] D. Sunuwar, S. Kim, and Z. Reyes, "Is 30 MHz enough for C-V2X?" in *Proc. IEEE 98th Veh. Technol. Conf. (VTC-Fall)*, Oct. 2023, pp. 1–7.

[31] G. Cecchini, A. Bazzi, B. M. Masini, and A. Zanella, "Localization-based resource selection schemes for network-controlled LTE-V2 V," in *Proc. Int. Symp. Wireless Commun. Syst. (ISWCS)*, Aug. 2017, pp. 396–401.

[32] M. H. Bahonar, M. J. Omidi, and H. Yanikomeroglu, "Low-complexity resource allocation for dense cellular vehicle-to-everything (C-V2X) communications," *IEEE Open J. Commun. Soc.*, vol. 2, pp. 2695–2713, 2021.

[33] N. Decarli, A. Guerra, C. Giovannetti, F. Guidi, and B. M. Masini, "V2X sidelink localization of connected automated vehicles," *IEEE J. Sel. Areas Commun.*, vol. 42, no. 1, pp. 120–133, Jan. 2024.

[34] M. H. Bahonar and M. J. Omidi, "Distributed pricing-based resource allocation for dense device-to-device communications in beyond 5G networks," *Trans. Emerg. Telecommun. Technol.*, vol. 32, no. 9, p. e4250, Sep. 2021.

[35] J. Chen, Q. Yuan, H. Ding, X. Zhu, and S. Zhang, "Low-latency NOMA-enabled vehicle platoon resource allocation scheme: A deep deterministic policy gradient-based approach," *IEEE Commun. Lett.*, vol. 28, no. 11, pp. 2568–2572, Nov. 2024.

[36] J. Kim, D. G. Duguma, P. V. Astillo, H.-Y. Park, B. Kim, I. You, and V. Sharma, "A formally verified security scheme for inter-gNB-DU handover in 5G vehicle-to-everything," *IEEE Access*, vol. 9, pp. 119100–119117, 2021.
[37] H. Park, Y. Jang, and J.-W. Choi, "Latency analysis of 5G C-V2X real-time video transmission over different channel states," 2024.
[38] F. Mahmood, E. Perrins, and L. Liu, "Energy-efficient wireless communications: From energy modeling to performance evaluation," *IEEE Trans. Veh. Technol.*, vol. 68, no. 8, pp. 7643–7654, Aug. 2019.
[39] *Physical Layer Procedures for Data*, document TS 38.214, Version 18.4.0, 3GPP, 2024.
[40] W. Yuan and K. Nahrstedt, "Energy-efficient CPU scheduling for multimedia applications," *ACM Trans. Comput. Syst.*, vol. 24, no. 3, pp. 292–331, Aug. 2006.
[41] Y. Mao, C. You, J. Zhang, K. Huang, and K. B. Letaief, "A survey on mobile edge computing: The communication perspective," *IEEE Commun. Surveys Tuts.*, vol. 19, no. 4, pp. 2322–2358, 4th Quart., 2017.
[42] *Overall Description of Radio Access Network (RAN) Aspects for Vehicle-to-everything (V2X) Based LTE NR*, document TR 37.985, Version 18.0.0, 3GPP, 2024.
[43] *NR; Radio Resource Control (RRC); Protocol Specification*, document TS 38.331, Version 18.4.0, 3GPP, 2024
[44] *5G; NR; Medium Access Control (MAC) Protocol Specification*, document TS 38.321, Version 18.4.0, 3GPP, 2024.
[45] *User Equipment (UE) Radio Transmission and Reception*, document TR 36.785, Version 14.0.0, 3GPP, 2016.
[46] J. Lagos, P. Renukaswamy, N. Markulic, E. Martens, and J. Craninckx, "A single-channel, 1-GS/s, 10.91-ENOB, 81-dB SFDR, 9.2-fJ/conv.-step, ringamp-based pipelined ADC with background calibration in 16nm CMOS," in *Proc. IEEE Symp. VLSI Technol. Circuits (VLSI Technol. Circuits)*, Jun. 2024, pp. 1–2.
[47] D. Hui, S. Sandberg, Y. Blankenship, M. Andersson, and L. Grosjean, "Channel coding in 5G new radio: A tutorial overview and performance comparison with 4G LTE," *IEEE Veh. Technol. Mag.*, vol. 13, no. 4, pp. 60–69, Dec. 2018.
[48] *NR; Multiplexing Channel Coding*, document TS 38.212, Version 18.3.0, 3GPP, 2024.
[49] *User Equipment (UE) Conformance Specification; Radio Transmission and Reception; Part 1: Range 1 Standalone*, document TS 38.521-1, Version 18.3.0, 3GPP, 2024.
[50] Q. Fu, J. Liu, J. Wang, and J. Mat, "Security-reliability tradeoff for hybrid automatic repeat request-assisted NR V2X communication," in *Proc. IEEE Wireless Commun. Netw. Conf. (WCNC)*, Apr. 2024, pp. 1–6.
[51] L. Buccheri, S. Mandelli, S. Saur, L. Reggiani, and M. Magarini, "Hybrid retransmission scheme for QoS-defined 5G ultra-reliable low-latency communications," in *Proc. IEEE Wireless Commun. Netw. Conf. (WCNC)*, Apr. 2018, pp. 1–6.
[52] A. Ahmed, A. Al-Dweik, Y. Iraqi, H. Mukhtar, M. Naeem, and E. Hossain, "Hybrid automatic repeat request (HARQ) in wireless communications systems and standards: A contemporary survey," *IEEE Commun. Surveys Tuts.*, vol. 23, no. 4, pp. 2711–2752, 4th Quart., 2021.
[53] *Study Channel Model for Frequencies From 0.5 To 100 GHz*, document TS 38.901, Version 18.0.0, 3GPP, 2024.
[54] *Study on Evaluation Methodology of New Vehicle-to-Everything (V2X) Use Cases for LTE and NR*, document TR 37.885, Version 15.3.0, 3GPP, 2019.
[55] MathWorks Inc. *5G Toolbox*. Accessed: Oct. 25, 2024. [Online]. Available: https://www.mathworks.com/products/5g.html
[56] MathWorks Inc. *Communications Toolbox*. Accessed: Oct. 25, 2024. [Online]. Available: https://www.mathworks.com/products/communications.html
[57] Y. Tew and K. Wong, "An overview of information hiding in H.264/AVC compressed video," *IEEE Trans. Circuits Syst. Video Technol.*, vol. 24, no. 2, pp. 305–319, Feb. 2014.
[58] *Series H: Audiovisual and Multimedia Systems; Infrastructure of Audiovisual Services-Coding of Moving Video*, ITU-T, Geneva, Switzerland, 2017.
[59] G. J. Sullivan, J.-R. Ohm, W.-J. Han, and T. Wiegand, "Overview of the high efficiency video coding (HEVC) standard," *IEEE Trans. Circuits Syst. Video Technol.*, vol. 22, no. 12, pp. 1649–1668, Dec. 2012.
[60] Z.-N. Li, M. S. Drew, and J. Liu, *Fundamentals Multimedia* (Texts in Computer Science). Cham, Switzerland: Springer, 2021.
[61] *C-V2X Use Cases, Methodology, Examples Service Level Requirements*, 5GAA, Berlin, Germany, 2021.
[62] *C-V2X Use Cases Service Level Requirements*, 5GAA, Berlin, Germany, 2023.
[63] Intel Corp. *Intel Core I7-8700K Processor (12 M Cache, Up To 4.70 GHz)*. Accessed: Sep. 23, 2024. [Online]. Available: https://www.intel.com/content/www/us/en/products/sku/126684/intel-core-i78700k-processor-12m-cache-up-to-4-70-ghz/specifications.html

HANYOUNG PARK (Graduate Student Member, IEEE) received the B.S. degree in electronics engineering from the School of Undergraduate Studies, Daegu Gyeongbuk Institute of Science and Technology (DGIST), Daegu, South Korea, in 2024. He is currently pursuing the M.S. degree with the Department of Electrical Engineering and Computer Science, DGIST. His research interests include communication theory, wireless communication, signal processing, and integrated sensing and communication (ISAC).

YONGJAE JANG (Graduate Student Member, IEEE) received the B.S. degree in electronics engineering from Kyung-Hee University (KHU), Yongin-si, Gyeonggi-do, South Korea, in 2017. He is currently pursuing the M.S. degree with the Department of Electrical Engineering and Computer Science, Daegu Gyeongbuk Institute of Science and Technology (DGIST), Daegu, South Korea. From 2018 to 2023, he was with SEMES Company Ltd., Cheonan, South Korea, a semiconductor equipment manufacturer, where he was a Global Customer Engineer with the ETCH Team. His research interests include vehicle-to-everything communication and autonomous driving.

KANGHYUN KO received the B.S. degree in electronics engineering from Handong University, Pohang, South Korea, in 2024. He is currently pursuing the M.S. degree with the Department of Electrical Engineering and Computer Science, Daegu Gyeongbuk Institute of Science and Technology (DGIST), Daegu, South Korea. His research interests include in-vehicle networks and high-speed wired communication.

JI-WOONG CHOI (Senior Member, IEEE) received the B.S., M.S., and Ph.D. degrees in electrical engineering from Seoul National University (SNU), Seoul, South Korea, in 1998, 2000, and 2004, respectively. From 2004 to 2005, he was a Postdoctoral Researcher with the Inter-University Semiconductor Research Center, SNU. From 2005 to 2007, he was a Postdoctoral Visiting Scholar with the Department of Electrical Engineering, Stanford University, Stanford, CA, USA. He was also a Consultant with GCT Semiconductor, San Jose, CA, USA, for the development of mobile TV receivers, from 2006 to 2007. From 2007 to 2010, he was with Marvell Semiconductor, Santa Clara, CA, USA, as a Staff Systems Engineer for next-generation wireless communication systems, including WiMAX and LTE. Since 2010, he has been a Professor with the Department of Electrical Engineering and Computer Science, Daegu Gyeongbuk Institute of Science and Technology (DGIST), Daegu, South Korea. His research interests include wireless communication theory, signal processing, biomedical communication applications, and brain–machine interfaces.